Journal of Applied Remote Sensing, Volume 13, Issue 1, 2019, Article number 016504
DOI:10.1117/1.JRS.13.016504

Implications of spectral and spatial features to improve the identification of specific classes

Akhil Kallepalli[a,*], Anil Kumar[b], Kourosh Khoshelham[c], David B James[a], Mark A Richardson[a]
[a]Centre for Electronic Warfare, Information and Cyber, Cranfield University, Defence Academy of the United Kingdom, Shrivenham, SN6 8LA UNITED KINGDOM
[b]Photogrammetry and Remote Sensing Department, Indian Institute of Remote Sensing, ISRO, Govt. of India, 4, Kalidas Road, Dehradun- 248001 INDIA
[c]Department of Infrastructure Engineering, University of Melbourne, AUSTRALIA

Abstract. Dimensionality is one of the greatest challenges when deciphering hyperspectral imaging data. Although the multi-band nature of the data is beneficial, algorithms are faced with a high computational load and statistical incompatibility due to the insufficient number of training samples. This is a hurdle to downstream applications. The combination of dimensionality and the real-world scenario of mixed pixels, the main challenges with imaging data are identification and classification. Here we address the complications of dimensionality by using specific spectral indices from band combinations and spatial indices from texture measures for classification, in order to better identify the classes. We classified spectral and combined spatial-spectral data and calculated measures of accuracy and entropy. A reduction in entropy and an overall accuracy of 80.50% was achieved when using the spectral-spatial input, compared to 65% for the spectral indices alone and 59.50% for the optimally determined principal components.

Keywords: hyperspectral imaging, vegetation analysis, classification algorithms, mixed pixels, urban scene classification.

***Corresponding author: Akhil Kallepalli a.kallepalli@cranfield.ac.uk

1 Introduction

A targets spectral information can be acquired in many, contiguous bands of specific wavelengths, a phenomenon known as hyperspectral imaging[1,2] Due to the nature of the information acquired (specific, narrow bandwidths detecting minor changes of reflectance), the datasets usually have intrinsic diagnostic characteristic with respect to the target.[3,4] The identification of targets can be achieved using variations in spectral responses that can be attributed to situational, conditional or illumination changes.

Most hyperspectral applications and assessments begin by addressing the dimensionality of the dataset. Spectral information is reduced using a pre-processing method to either identify features

on the basis of interest or 'project' them into a feature space based on the amount of valuable information. Even when attributing credibility to the narrow-bandwidth, contiguous bands for greater spectral information, the datasets also encounter the "curse of dimensionality." Usually referred to as the Hughes Phenomenon,[5] the statistical accuracy of class recognition is known to optimise for a subset of bands and subsequently decline due to inadequate training samples.[6] The benefits of dimensionality reduction including the lower computational load are widely accepted.[1,3,7]

Extending the current literature, we gain insight into the implications of using spectral and spatial information as the input database for the classification algorithm instead of an output of feature extraction. This paper reports the results of knowledge-based feature selection and transformation to indices for the improvement of identification for specific classes. A possibilistic *c*-means (PCM) classifier was used due to its advantages over other mixed pixel classifiers, i.e. the probability of classes within a pixel are not constrained. We applied the classifier to the Airborne Prism EXperiment (APEX) Open Science Dataset (OSD). To demonstrate the improvement in the identification accuracy of individual classes, a baseline classification was established using principal component analysis (PCA) dimensionality reduction to establish entropy for the statistical quantification of uncertainty.[6] The classification approach is based on our earlier report[8] and targeted the identification of specific, individual classes and the improvements were used to validate the results.

2 Related Work

Like many types of imaging information, hyperspectral data has many applications including its use determine the extent of vegetation for health analysis,[9] species-level classification[10] and biomedical research.[11] However, the additional spectral information reduces the classification accuracy, and results in a high computational load. This phenomenon has been described as a statis-

tical inadequacy of training samples compared to the number of bands in the dataset.[5] A 'peaking phenomenon' was said to occur, with accuracy improving for a subset of bands and thereafter declining with every additional band. Although this phenomenon has been challenged as apparent in nature,[12] the reduction of hyperspectral data dimensionality is nevertheless a key step in the application of imaging data. In order to avoid the problems associated with dimensionality, numerous methods have been applied for feature extraction, including the use of orthogonal subspace projections,[7] PCA,[13,14] Minimum Noise Fraction (MNF),[15] and morphological transformations.[16]

Information from higher-dimensional imaging data requires methods that can broadly be categorized as feature selection and feature extraction. Feature selection methods refer to algorithms that output a subset of the original dimensionality, whereas feature extraction methods create new features either by transformation or by combining input features.[17] Methods such as PCA use linear transformation to convert the data into a reduced or "intrinsic dimensionality",[18] such transformations are not universally applicable. An attempt has been made to optimise the accuracy of the feature selection method by using sequential forward selection, steepest ascent and fast constrained search strategies.[19] Another approach attempted simultaneously to reduce the dimensionality and classify the dataset by projecting the signals into orthogonal subspace, eliminating unwanted signatures and improving signal-to-noise ratios.[7] In another, a sequence of morphological transformations was use to filter and classify highly-dimensional data.[16] As well as reducing the computational load, dimensionality reduction greatly improves the classification accuracy. It results in a comparable number of training samples against a subset of bands with the information from the original image. However, PCA and similar methods have several disadvantages: they assume the data dimensionality can be reduced by linear transformation when data could be non-linear in relation, and the initial components are dominated by data showing greater variance while

not (with exceptions) maximising the extracted information.[13] These disadvantages have prompted further research into non-linear and/or knowledge-based dimensionality reduction.

2.1 Pixel-based Spectral Indices

Emphasising the importance of obtaining useful information from the image data, methods of feature selection can be employed or combinations of bands (feature extraction) can be used. Spectral indices are derived from distinctive characteristics in the spectral signatures of the target in order to highlight them against the background. For example, biophysical variables can be quantified by remote sensing,[20] introducing greyscale and colour signatures of features.[21–23] The formulation of spectral indices began with the simple ratio (SR)[24] of bands. The contrasting spectral response (Figure 1) in the infrared (0.8 μm) and red (0.675 μm) wavelength regions was used by defining the ratio of individual pixel values.

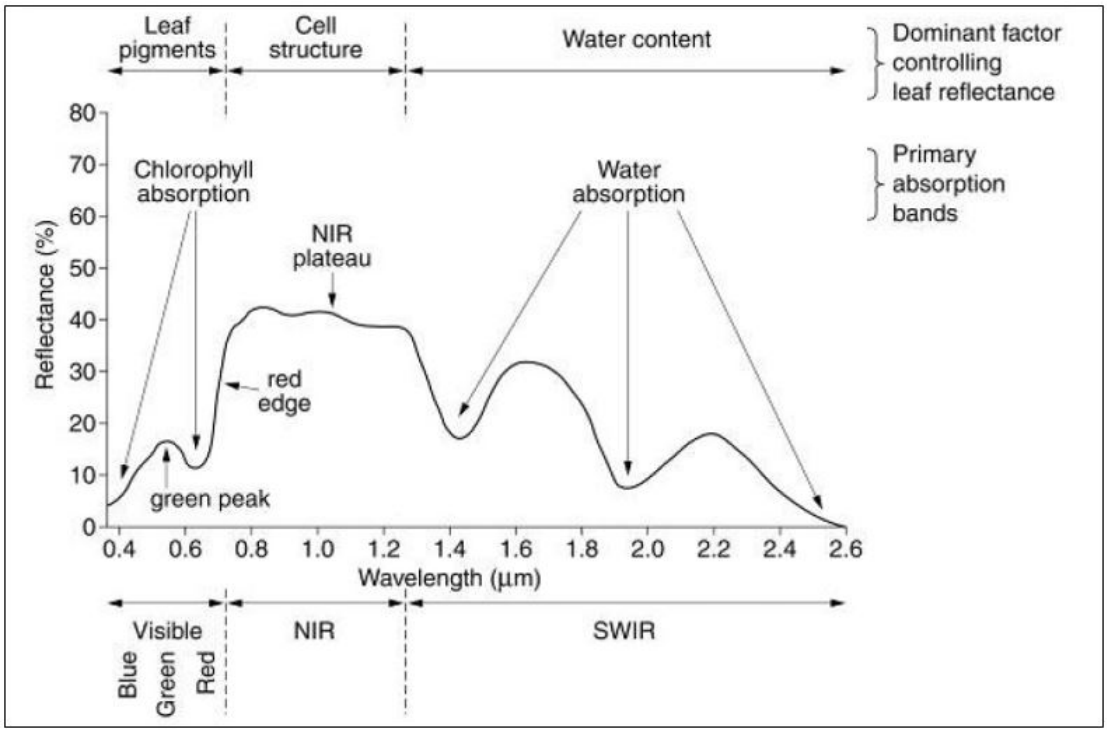

Fig 1 Identifiable biophysical aspects correlated with spectral information.[25]

One of the most popular spectral indices is the normalised difference vegetation index (NDVI),[26] which is a modified version of the SR index. The ratio of the reflectance values (R) in the near-infrared and red bands ($(R_{NIR} - R_R)/(R_{NIR} + R_R)$ for Landsat 1 data) was applied in NDVI to enhance vegetation features compared to the background, producing results in greyscale values.[27] Although the delineation of vegetation features by NDVI was satisfactory, the correlation between different vegetation parameters and the underlying soil reflectance affect the results.[28] To address these vegetation-specific aspects, many indices have been formulated to account for the chlorophyll content,[29–31] Leaf Area Index (LAI),[32–34] and other parameters.

Interference caused by the soil were addressed by the development of the Soil Adjusted Vegetation Index (SAVI), which is shown in Equation 1.[28]

$$SAVI = \frac{(R_{NIR} - R_R)}{(R_{NIR} + R_R + L)} \times (1 + L) \tag{1}$$

where L defines the prior knowledge of the vegetation density, i.e. low vegetation ($L = 1$), intermediate vegetation cover ($L = 0.5$) and high density vegetation cover ($L = 0.25$). The need for prior knowledge of vegetation density cover was eliminated in the modified SAVI index (MSAVI)[35] which is shown in Equation 2.

$$MSAVI = 0.5(2R_{NIR} + 1 - \sqrt{(2R_{NIR} + 1)^2 - 8(R_{NIR} - R_{Red})}) \tag{2}$$

The implications of narrowband data vs broadband data have been considered when estimating LAI and green cover.[36] Applying the basic understanding of chlorophyll absorption in the red wavelength region and reflectance at NIR wavelengths,[37] previously defined vegetation indices

were explored to highlight the importance of narrow band hyperspectral imagery. LAI and canopy chlorophyll density (CCD) were investigated using previously defined indices.[38]

The chlorophyll absorption in reflectance index (CARI)[39] was improved by developing a modified version (MCARI)[34] which compares the reflectance at 0.67 to 0.55 μm and 0.7 μm as shown in Equation 3.

$$\textit{MCARI} = [(R_{0.7} - R_{0.67}) - 0.2(R_{0.7} - R_{0.55})] \times \frac{R_{0.7}}{R_{0.67}} \tag{3}$$

The diagnostic capability of spectral indices and narrowband imaging were further highlighted through improved pigment and chlorophyll estimation[40,41] in open-canopy tree crops,[42] and viticulture,[43,44] and by measuring physiological characteristics using the physiological reflectance index (PRI),[45] , as well as the accumulation of specific metabolites such as carotenoids.[46]

The application of mathematical and/or ratio-based spectral indices to enhance certain features was also applied beyond the analysis of vegetation. The normalised difference built-up index (NDBI)[47] was developed to classify built-up parts of urban areas utilising the broadband data from the Landsat Thematic Mapper, as shown in Equation 4.

$$\textit{NDBI} = \frac{(R_{TM5} - R_{TM4})}{(R_{TM5} + R_{TM4})} \tag{4}$$

where $TM5$ is the shortwave infrared-1 band (1.55–1.75 μm) and $TM4$ is the NIR band (0.76–0.90 μm) of the Landsat Thematic Mapper.

Water bodies have been identified via their infrared absorption properties using the normalised

difference water index (NDWI)[48] as shown in Equation 5.

$$NDWI = \frac{(R_{0.86} - R_{1.24})}{(R_{0.86} + R_{1.24})} \tag{5}$$

2.2 Texture-based Spatial Indices

Although spatial indices can be interpreted in many ways,[8] current research focusses on utilising the spatial variation of pixels and the influence of a neighbourhood of pixels on the detection of targets. Spatial textures are used to discriminate spectrally-similar targets and are therefore applied to the spectral index output(s).

The primary pattern elements are spectral, textural and contextual features.[8] Whereas early research focused on the coarseness of features and edge definition, a discussion of textural features identified the important influence of pixel neighbourhoods.[21] Derived textures used angular nearest neighbourhood grey-tone spatial dependence matrices.[21,49] The neighbourhood of the pixels depend on the variation across pixels in the image. This correlates with the resolution of the image data and the extent of the targets. For example, if a large neighbourhood is considered for a much smaller target (e.g. house roofs, as used in the current study), the target is lost in the larger window of texture calculation. Alternatively, larger neighbourhoods can be considered for targets (vegetation) that occupy a larger area of the image and show less spatial variation.

Texture is important for the accurate interpretation of images[22] (Figure 2). Applications have expanded to the interpretation of synthetic aperture radar (SAR) imagery using grey-tone co-occurrence textural matrices.[50] However, the most suitable texture analysis elements should be selected rather than using all elements, and this is the approach we have followed.

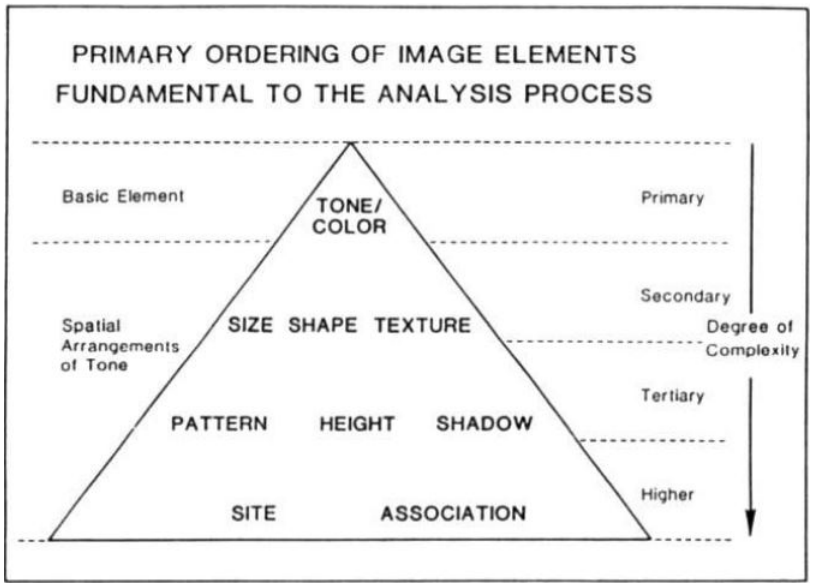

Fig 2 Priority ordering of image elements, the basis of image analysis procedures[22]

Texture analysis can provide quantitative discriminators along with spatial metrics,[49] in order to improve the identification of spatial information from datasets. We set out to improve the classification accuracy of datasets when using spatial and spectral information together as input to the classifier for identification of specific classes.

3 Methods

Many methods for the assessment of hyperspectral imaging for classification purposes perform dimensionality reduction before employing a classifier for target identification.[1,3,7,14,16,51] The need for a versatile airborne imaging system resulted in the European Space Agency (ESA) APEX project funded by Switzerland and Belgium.[6,52] Detailed information about the APEX project can be found elsewhere.[52–54]

The APEX instrument operates in the range 0.38–2.5 μm and can collect data in 313 freely configurable bands.[55] The APEX OSD is freely available online (http://www.apex-esa.org/content/free-

data-cubes). Raw data acquired by the sensor in June 2011 was processed to a Level 1 processed dataset.[56] The spectral and spatial resolutions are 285 bands and 1.8 metres respectively. The captured dataset included a variety of targets including grass, forests, roofs and roads. The classes were identified using the SwissTopo web portal[57] and specific pixels and regions of interest were shared by the data providers. The classes investigated were (1) Artificial Turf; (2) Black Roof; (3) Building; (4) Clay Soil; (5) Grass; (6) Lawn Tennis Court; (7) Coniferous Forest; (8) Deciduous Forest; (9) Pasture; (10) Railway; (11) Red Roof; (12) Red Synthetic Ground; (13) Road; (14) Roofs; (15) Sand; (16) Stressed Grass; (17) Synthetic Sports Surface; (18) Vineyard; (19) Water and (20) Yellow Tartan. Training and testing datasets were developed and denoted in Figure 4.

The 'baseline' classification using PCA for dimensionality reduction was used to provide a means of comparison with the indices-based method.[8] Entropy measures were used to ascertain the minimum number of principal components needed for classification. When more than seven components were present, there was no significant increase in classification accuracy to justify the increase of number of input bands to the PCM classifier. The classification and the accuracy assessment of the baseline classification (Figure 3) were therefore achieved using seven components, establishing the overall baseline accuracy of 59.50%.

The spectral signatures of each type of forest were similar, due to the presence of vegetation, but varied in terms of intensity (Figure 5). This variation was caused by difference of physical structure of coniferous and deciduous leaves, the latter having a larger surface area, and thus higher reflectance. Similar observations were recorded when comparing other classes (Figure 6).

There were key differences in the spectral responses of healthy and stressed grass. The red edge represents absorption by leaf pigments and reflectance based on cell structure. The lack of leaf pigments in stressed grass contributes to the poorly-developed red edge. When comparing the

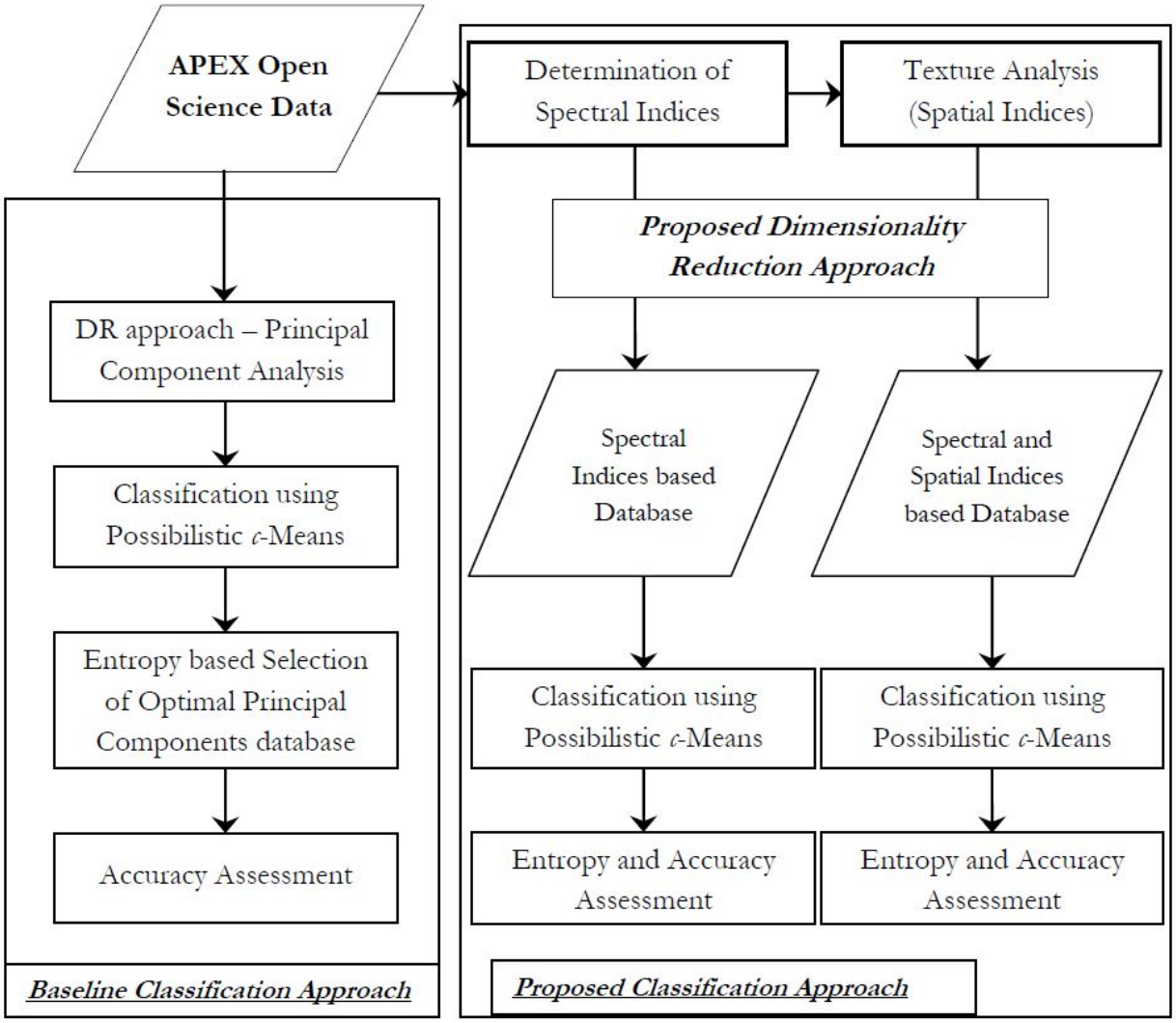

Fig 3 The methodology followed in the study is presented. We would like clarify that the proposed dimensionality reduction approach in this study is the knowledge-based identification of hyperspectral bands that will be used to evaluate the spectral indices. These identified spectral and spatial indices will be used as input to the classification algorithm.

sports surfaces (Figure 7), the Red Sports Surface shows distinguishable characteristics at ≈ 0.8 μm when the spectral curve (shown in red) shows reflectance whereas the other two surfaces show absorption.

The reduction of reflectance and shift of red edge position (REP) towards the red wavelengths is indicative of less absorption by chlorophyll. The REP is estimated using the first derivative of the spectral response as a function of reflectance, yielding a specific band number of the red edge.[59]

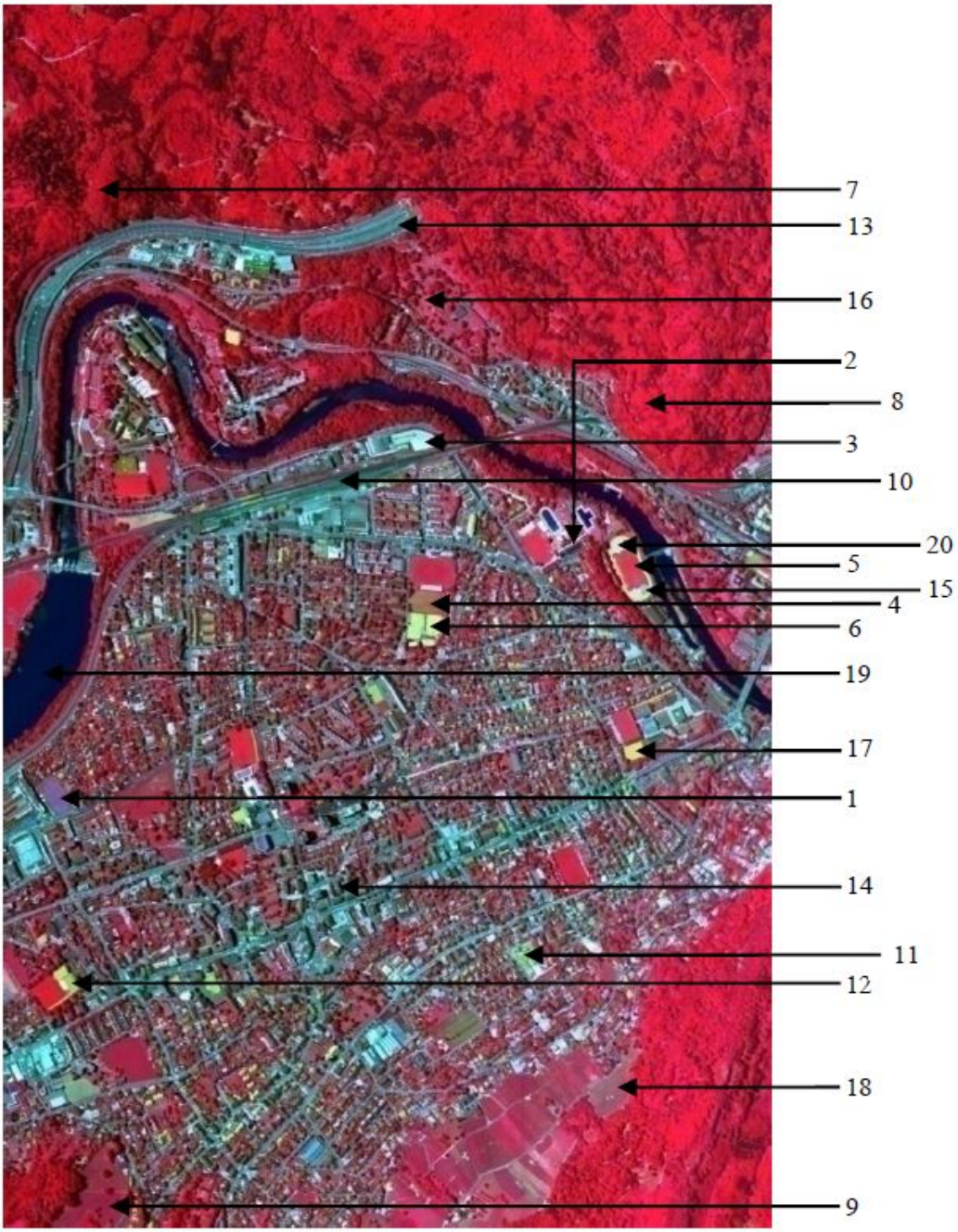

Fig 4 Airborne Prism EXperiment (APEX) Open Science Data (OSD) false colour composite (FCC) image of Baden, Switzerland,[58] showing representative areas of the different classes in the study.

The spectral curve of Stressed Grass illustrates a poorly defined red edge (Figure 8) with the first derivative of the spectral curve indicating a shift of REP (Figure 9) compared to the typical red edge for Grass and the position of the red edge peak at the 64th band (Figure 9).

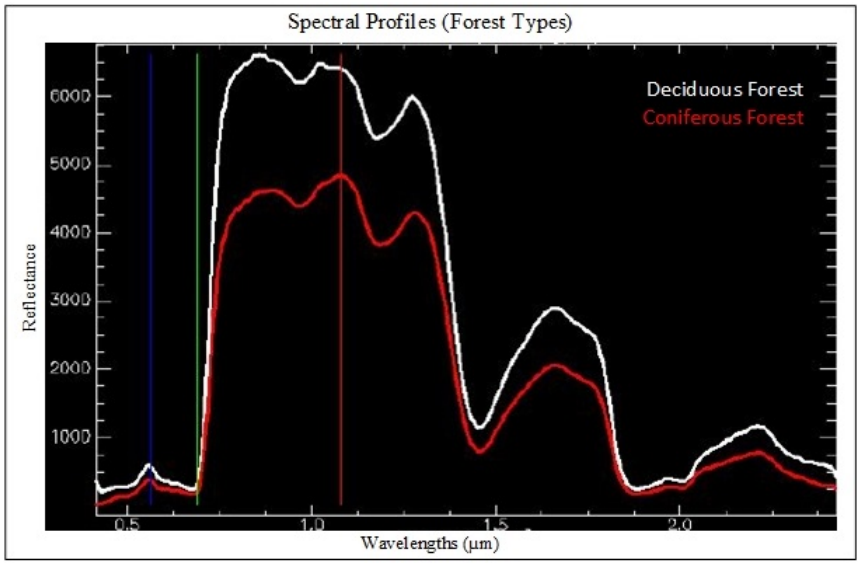

Fig 5 Spectral response of Deciduous and Coniferous forests

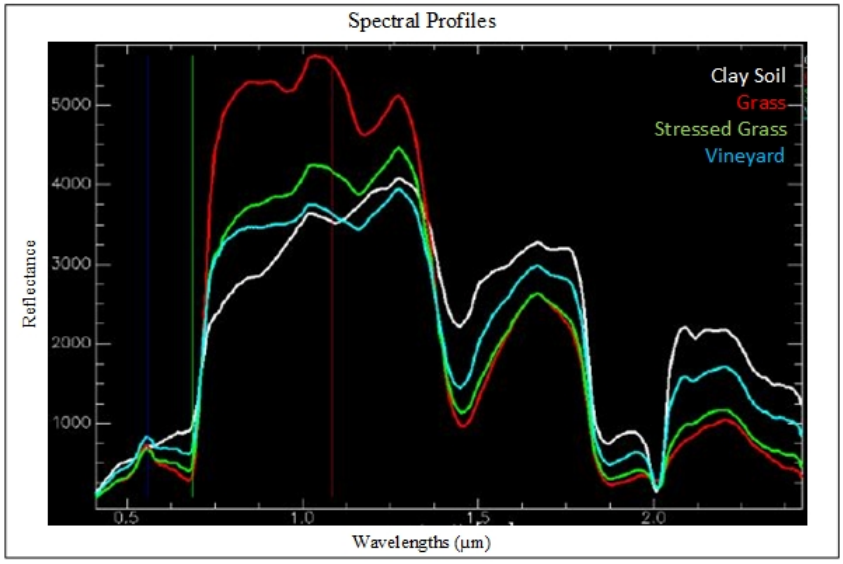

Fig 6 Spectral response of Soil, Grass, Stressed Grass and Vineyards

3.1 Classification Approach

When image data are collected from a target, the pixel is not composed of a single class in every situation. When more than one class is present in a single pixel, it is considered to be 'mixed'. Classifiers that constrain a pixel to a single class are not suitable for the classification of mixed pixels. Soft or fuzzy classification approaches are better suited to such cases because they esti-

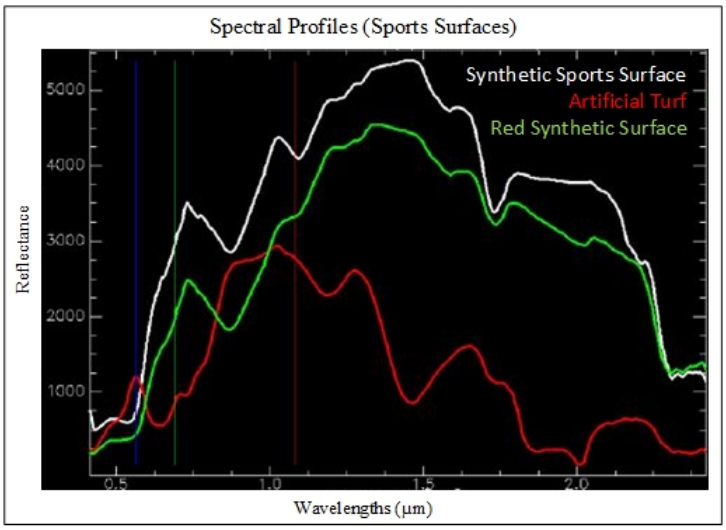

Fig 7 Spectral response of Synthetic Sports Surface, Artificial Turf and Red Synthetic Ground

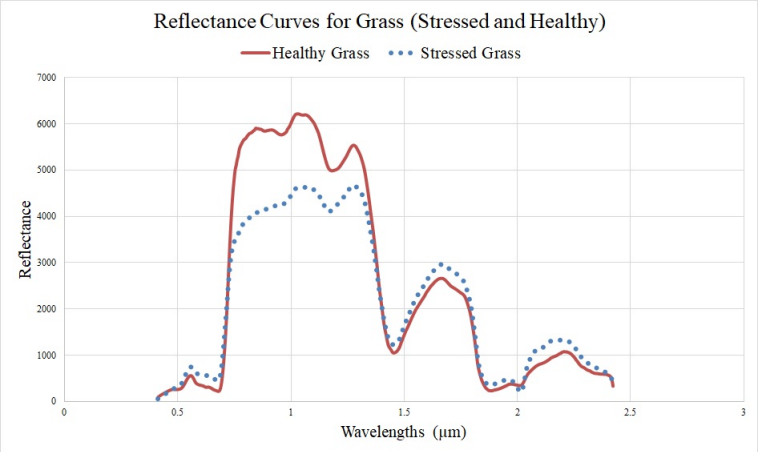

Fig 8 Reflectance curves of Healthy Grass and Stressed Grass showing the variation of the NIR plateau, indicating that the chlorophyll concentration in the leaf declines under stress.

mate the probability of a pixel belonging to a class, allowing multiple classes to have a degree of presence in a single pixel.

Fuzzy *c*-means (FCM) and possibilistic *c*-means (PCM) algorithms were considered for classification but FCM was not suitable for this application because it only achieves dependable accuracy when all the classes are exhaustively defined (the membership function of the classifier is constrained to 1). In contrast, due to the lack of a membership function constraint, the PCM clas-

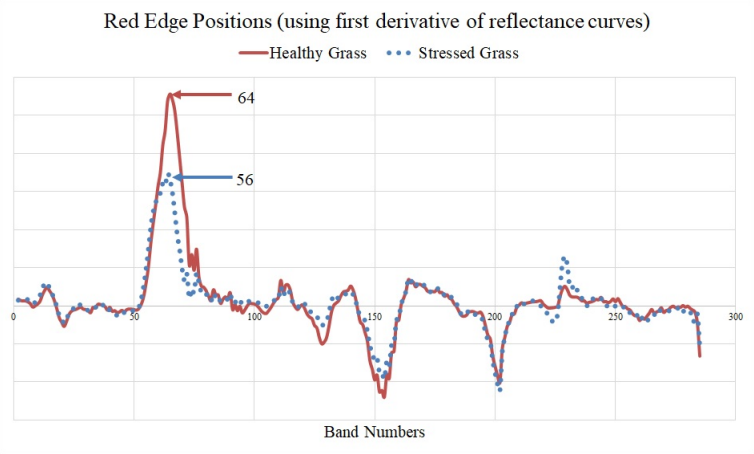

Fig 9 The red edge position (REP) shifts towards the red wavelengths when the amount of chlorophyll in vegetation declines. The shift is indicative of the health of the vegetation, which is grass in this case.

sifier better evaluates the presence of the class in a pixel as a function of its signature without the constraints of other classes.[60] In the case of PCM, the membership function of each class is defined using the following constraints (Equations 6 –8.[60,61]

$$u_{ij} \in [0,1] \; for \; all \; i \; and \; j \tag{6}$$

$$0 < \sum_{j=1}^{n} u_{ij} \leq \; N \; for \; all \; i \tag{7}$$

$$max_i \; u_{ij} > 0 for \; all \; j \tag{8}$$

where u_{ij} is the membership value of pixel x_i belonging to a class β_i; and N is the number of pixels (or feature points).

3.2 Spectral Indices

Spectral inferences about the classes were made by using identification 'keys' or specific bands that allow the classifier to distinguish between targets. These keys are contrasting spectral behaviour of absorption and reflection (troughs and peaks) in the spectral curve. The spectral properties of all the identified classes were compared. Table 1 shows the identifiable properties and their corresponding wavelength regions for the vegetation features. Using this method of feature selection, we reduced the dimensionality of the hyperspectral dataset to bands with the most appropriate information, so we consider this to be a knowledge-based dimensionality reduction approach. The bands selected in this process form the input database for the classifier.

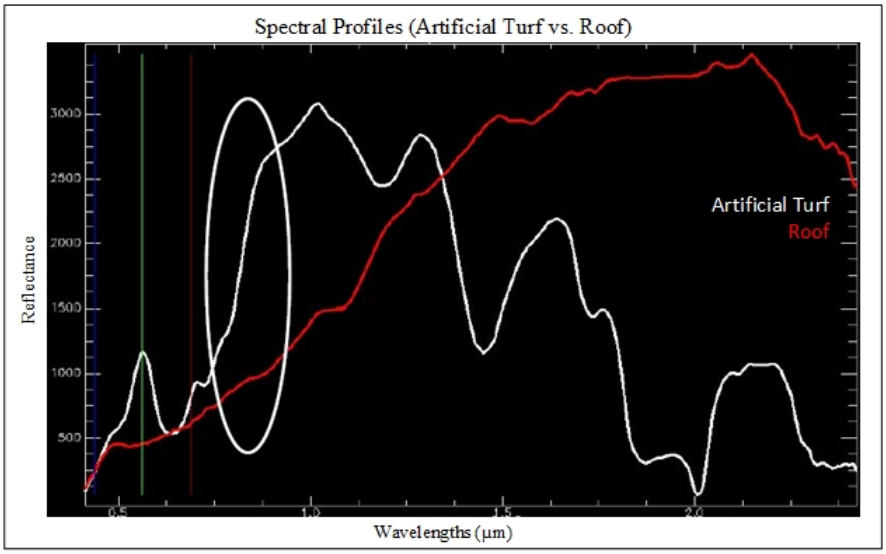

Fig 10 Spectral Curve comparison of Artificial Turfs and Roofs

Following the identification of keys with the necessary spectral information, spectral indices were defined using band combinations (Table 2). The indices did not always uniquely identify a specific class, e.g. the increase in reflectance for Artificial Turf and Roof spectral curves (indicated in Figure 10). Therefore, when spectral indices are defined in these regions, both classes are

highlighted. Such conflicts among the 20 classes considered in this study are listed in Table 3.

Table 1 Correlations between wavelength regions and their biological significance[62–64]

Wavelength Region	**Wavelength (λ)**	**Band Description and Significance**
Blue	0.49 μm	Sensitive to loss of chlorophyll, browning, ripening, senescence and soil background effects. Also sensitive to carotenoid pigments.
Green 1	0.52 μm	Maximum "positive change in reflectance per unit variation in wavelength" of visible spectrum is seen around this green wavelength and is sensitive to pigment content
Green 2	0.55 μm	Green peak in the visible spectrum; strongly related to chlorophyll content.
Green 3	0.575 μm	Maximum "negative change in reflectance per unit variation in wavelength" of visible spectrum is seen around this green wavelength and is sensitive to pigment content.
Red 1	0.66 μm	Chlorophyll absorption pre-maxima (reflectance minima - 1)
Red 2	0.675 μm	Chlorophyll absorption maxima. Greatest soil-crop contrast seen at this wavelength.
Red edge - 1	0.7 μm	Chlorophyll absorption post-maxima (reflectance minima - 2). This point marks the change of maximum red-absorption to dramatic increase in red reflectance along the red edge. This has been found to be sensitive to stress levels in vegetation.
Red edge - 2	0.72 μm	Critical point on the red edge where the "maximum change of slope reflectance spectra per unit change in wavelength" occurs. Sensitive to temporal changes in crop growth, stress, etc.
NIR	0.845 μm	Centre of the "NIR shoulder". Strongly correlated to chlorophyll.
NIR Peak - 1	0.905 μm	Peak of the NIR spectrum. Sensitive to stress or growth stages of some crops, where there is a significant change in reflectance along the NIR shoulder. Useful for calculating crop moisture sensitive index.
NIR Peak - 2	0.920 μm	Peak of the NIR spectrum
NIR - Moisture Sensitive	0.975 μm	Centre of moisture-sensitive portion of NIR. Various measures of plant moisture can be made from this wavelength's reflectance.

Table 2 Spectral indices database chosen for classification input; 20 classes are identified in these indices, as some indices identify more than 1 class. Note that the band numbers correspond to APEX OSD data

Object Class	Formulated/Applied Index	APEX Band Combination
Artificial Turf	Band Ratio	95, 76 (0.8752 μm, 0.7716 μm)
Black Roof	Band Ratio	160, 149 (1.45 μm, 1.343 μm)
Buildings	NDBI	160, 145 (1.45 μm, 1.304 μm)
Clay Soil	Band Ratio	236, 225 (2.09 μm, 2.007 μm)
Coniferous Forest	Band Ratio	85, 53 (0.8167 μm, 0.6816 μm)
Deciduous Forest	MTVI1	81, 17, 52 (0.7958 μm, 0.5567 μm, 0.6784 μm)
Red Synthetic Ground	Band Ratio	197, 192 (1.782 μm, 1.74 μm)
Stressed Grass	Band Ratio	234, 226 (2.074 μm, 2.015 μm)
Vineyard	Modified NDVI (devised from spectral curve behaviour in SWIR)	236, 225 (2.09 μm, 2.007 μm)
Water	NDWI	183, 146 (1.662 μm, 1.314 μm)
Roof	Band Ratio	142, 122 (1.275 μm, 1.082 μm)
Basic Vegetation Index	MSAVI	85, 53 (0.8167 μm, 0.6816 μm)

Table 3 Conflicting classes from identified spectral keys

Object class-specific index	Additional Classes Identified
Artificial Turf	Roof
Black Roof	Water
Buildings	Multiple classes
Clay Soil	Artificial Turf, Vineyards
Coniferous Forest	-
Deciduous Forest	Grass
Red Synthetic Ground	Multiple Classes
Stressed Grass	Clay Soil, Vineyard
Vineyard	Clay Soil, Stressed Grass
Water	-
Roof	-
Basic Vegetation Index	All vegetation in the study area

3.3 Spatial Indices from Texture Analysis

The class-specific feature extraction of the spectral characteristics provided us with the second input database (the first being the input of principal components[6]) for the classifier. However,

when dealing with classes that have comparable spectral behaviour (e.g. forests and grass), spatial distribution would act as a distinguishing factor. Therefore, texture analysis (neighbourhood distribution) was considered for the purpose of exploiting the spatial distribution of the classes.

Grey-Level Co-occurrence Matrix (GLCM) texture analysis has been described in detail.[21] The texture measurement involves the selection of a neighbourhood of pixels followed by quantifying the grey-level variation to identify the most appropriate textural feature. The analysis is performed on the spectral indices output, in order to distinguish between spectrally similar targets. The choice of neighbourhood for the pixels is dependent on the spectral resolution of the image data and the extent of the target. Smaller targets that span a few pixels require smaller windows of texture analysis, whereas larger targets benefit from the flexibility of larger spectral windows. After considering the available texture measures, we chose the following (Equations 9 – 11).

$$Mean\ (\mu_i) = \sum_{i,j=0}^{N-1} i\ (P_{i,j})\ \ ;\ \ Mean\ (\mu_j) = \sum_{i,j=0}^{N-1} j\ (P_{i,j}) \tag{9}$$

$$Entropy\ = \sum_{i,j=0}^{N-1} P_{i,j}\ (-ln\ P_{i,j}) \tag{10}$$

$$Second\ Moment = \sum_{i,j=0}^{N-1} (P_{i,j})^2 \tag{11}$$

where $P_{i,j}$ is the $(i,j)^{th}$ entry in the grey tone spatial dependence matrix and N is the number of grey levels in the quantised image.

We initially tested multiple window sizes and choice of the neighbourhood was dependent on the spatial extent of the classes. Thus, classes such as Roof did not need window sizes larger than

3x3. Due to variations in the extent of vegetation across the image, larger window-sizes could be accommodated and provided better results. The chosen spatial indices (Table 4) were added to the spectral indices to make up the third input for classification.

Table 4 Selected texture measures (spatial indices) for input to the classifier

Source Index	Texture	Window size (Neighbourhood)
Black Roof	Entropy	3 x 3 window
Clay Soil	Mean	3 x 3 window
Coniferous Forest	Second Moment	3 x 3 window
MSAVI Vegetation Index	Second Moment	5 x 5 window
Roof	Mean	3 x 3 window

Vegetation classes benefit from using the second moment texture because the second moment generates better results when a few pixels in the neighbourhood are higher in intensity.

Entropy generates high output values when measured on neighbourhoods that have a continuous and consistent pixel values. The texture measure derives the desired output when applied to features such as Black Roof, which have a consistent distribution of pixel values. The mean distribution of pixel values highlights pixels of high intensity and increases the separability of classes such as Roof and Clay Soil.

The spectral indices input database and the combined spectral and spatial indices database were evaluated for classification accuracy using the PCM classifier and the results were compared to determine the suitability of the method. The primary motivation for this research was to better understand the implications of combining spectral and spatial information for the classification of the dataset, following entropy analysis and accuracy assessment after defuzzification.[6] The accuracy assessment includes:

1. User's Accuracy (UA) which is the reliability or probability that a pixel class on the image represents the same on the ground.

2. Producer's Accuracy (PA) which represents how well a certain area has been classified

3. Overall Accuracy (OA) which represents the number of pixels correctly classified when compared with ground truth and knowledge information.

4 Results

We selected the 12 spectral and 5 spatial input bands. Combinations of these were used to create the input database for classification. The results are presented in the order of baseline classification, followed by spectral indices alone, followed by a combination of texture features in addition to the spectral indices input. Entropy measures were not calculated in scenarios where classes were not identified and are shown using the symbol '/' in Tables 5 – 7.

The first inputs to the classifier were the principal components derived by PCA. The appropriate number of principal components was determined by entropy analysis.[6] The classification using these principal components yielded an overall accuracy of 59.50%. The second input to the classifier was the spectral indices database (12 features shown in Table 2). As well as improving the overall classification accuracy to 65% (Table 5), the spectral indices input database also identified seven classes that were previously unidentified when using the principal components alone. Entropy measures were calculated for an average of 50 membership vectors per class.

When comparing the indices input (Table 5) and the spectral-spatial indices (Table 6) for classification, we observed a decrease in entropy measures for the majority of the classes, inferring a reduction in the level of uncertainty when applying class labels to the pixels. Although the entropy was lower, the defuzzified outputs also achieved a lower classification accuracy of 62.50%. However, a significant improvement in classification accuracy was achieved for vegetation classes, such as Vineyard (Table 6).

Table 5 Entropy determination and classification results when using the optimally chosen principal components (7 PCs) and only the spectral indices as input for the classifier. The symbol '/' indicates that the class was not identified in the classification process.

Class	PC Input Database (7 features)			Indices Input Database (12 features)		
	Entropy	**UA**	**PA**	**Entropy**	**UA**	**PA**
Artificial Turf	/	20	100	1.94	100	100
Black Roof	/	62.5	83.34	/	55.56	100
Building	1.35	100	50	/	100	42.86
Clay Soil	1.334	88.89	80	1.45	90	100
Grass	/	40	44.45	/	40	57.14
Lawn Tennis Court	1.26	70	100	/	40	100
Coniferous Forest	1.3	60	40	1.62	80	57.14
Deciduous Forest	/	80	29.63	1.6	90	50
Pasture	/	30	100	1.46	55.56	100
Railway	/	28.57	100	/	30	50
Red Roof	1.1	100	25	/	66.67	54.55
Red Synthetic Ground	1.15	60	85.71	/	60	100
Road	0.86	90	47.37	/	70	23.34
Roof	/	40	50	0.68	100	66.67
Sand	1.23	50	100	/	10	100
Stressed Grass	/	40	40	1.49	70	70
Synthetic Sports Surface	/	100	100	/	44.45	100
Vineyard	1.07	30	50	1.49	66.67	75
Water	/	100	90.9	2.06	100	90.91
Yellow Tartan	/	33.34	100	0.6	30	100
Overall Classification Accuracy	**59.50%**			**65%**		

Although the addition of spatial indices improved the classification accuracy for specific individual classes (e.g. Synthetic Sports Surface, Pastures), the overall classification accuracy dropped below the 65% achieved when using spectral indices alone. Therefore, the assignment of spatial classes was investigated while using a total of 16 spatial indices (without MSAVI-based texture) and 15 (without MSAVI-based and Black Roof Entropy textures) while including all spectral indices (Table 2). The combination of 16 indices achieved the highest accuracy of 80.50% was achieved (Table 6) with better individual accuracies and lower degrees of uncertainty for classification.

Table 6 Entropy determination and classification results when using the Indices and Textures database (17 and 16 features) as input for the classifier. The symbol '/' indicates that the class was not identified in the classification process.

Class	Indices and textures (17 features)			Indices and textures without MSAVI-based texture (16 features)		
	Entropy	**UA**	**PA**	**Entropy**	**UA**	**PA**
Artificial Turf	1.146	80	80	1.274	100	100
Black Roof	/	37.5	75	/	12.5	100
Building	0.63	60	31.58	0.44	100	63.63
Clay Soil	1.212	80	100	1.2	100	100
Grass	1.004	60	85.71	1.25	90	90
Lawn Tennis Court	0.64	80	66.67	0.5	88.89	100
Coniferous Forest	0.956	100	71.43	1.34	100	83.33
Deciduous Forest	1.02	80	61.54	1.35	100	76.92
Pasture	0.966	71.43	83.34	1.25	44.44	100
Railway	/	10	33.34	/	25	100
Red Roof	/	20	100	0.46	100	91.67
Red Synthetic Ground	0.65	81.82	90	0.55	42.86	100
Road	/	50	15.625	0.44	88.89	24.24
Roof	/	30	27.27	/	71.43	75
Sand	/	20	33.34	/	14.29	100
Stressed Grass	1.126	80	80	1.3	87.5	100
Synthetic Sports Surface	0.65	50	100	0.55	87.5	100
Vineyard	0.94	80	88.89	1.1	90.91	83.34
Water	1.44	100	76.92	1.85	90	75
Yellow Tartan	/	10	100	0.5	33.33	100
Overall Classification Accuracy	**62.50%**			**80.50%**		

The defuzzification of the classification outputs assigns a class label of the highest membership to a considered pixel. Although a few classes were not identified by the PCM classifier, their results were measured after defuzzification through which every pixel was assigned a class label.

5 Discussions

Our results confirm that using spectral-spatial indices can improve the accuracy of classification. However, a key inference from the results is that not all spatial indices added valuable information to the database. The removal of MSAVI-based texture (Table 6) improved the overall classification

Table 7 Entropy determination and classification results when using the Indices and Textures database (15 features) as input for the classifier. The symbol '/' indicates that the class was not identified during the classification process.

Class	**Indices and textures without MSAVI-based and Black Roof Entropy (15 features)**		
	Entropy	**UA**	**PA**
Artificial Turf	1.296	100	100
Black Roof	/	30	100
Building	0.399	100	70.59
Clay Soil	1.14	100	100
Grass	1.17	80	80
Lawn Tennis Court	0.46	75	100
Coniferous Forest	1.18	100	83.33
Deciduous Forest	1.2	90	81.82
Pasture	1.19	70	100
Railway	/	12.5	33.33
Red Roof	0.44	63.64	70
Red Synthetic Ground	0.52	75	85.71
Road	0.41	73.33	28.95
Roof	/	72.73	66.67
Sand	/	0	0
Stressed Grass	1.16	100	63.64
Synthetic Sports Surface	0.54	75	100
Vineyard	1.1	50	100
Water	1.138	100	83.33
Yellow Tartan	0.5	11.12	100
Overall Classification Accuracy	**72%**		

accuracy of the dataset. This combination of knowledge-based feature selection and extraction for classification improves classification accuracy for specific classes, while intrinsically reducing the dimensionality of the hyperspectral dataset by choosing the information input to the classifier.

The baseline classification used a dimensionality-reduced input from the PCA to reduce the hyperspectral data to its intrinsic dimensionality of seven principal components. The achieved an accuracy of 59.50% and the lowest number of classes were successfully identified, and subsequently classified. The usage of spectral indices (Table 2), irrespective of the arising conflicts of classes (Table 3) improved the classification accuracy for the dataset. The knowledge-based selec-

tion of spectral information and the reduction of dimensionality using indices allowed the classifier to identify and classify the pixels with greater accuracy. The use of this spectral information improved the classification of vegetation classes (Coniferous Forest, Deciduous Forest, Pasture and Stressed Grass). Marginal improvement was also observed for the classification of Clay Soil and Artificial Turf.

Classes such as Black Roof, Grass and Synthetic Sports Surface remained unidentified when only the spectral information was used. Furthermore, the Railway class remained unclassified for all the spectral–spatial indices inputs. Due to its nature, the railway network is better identified using spatial information, so object oriented classification approaches may be more suitable for the classification of railway networks.

The identification of classes improved when spectral and spatial features were combined as the input database. Although the overall accuracy was lower when compared to the spectral indices input, the accuracy of classifying Grass, Coniferous Forest and Deciduous Forest improved. The entropy measure was substantially reduced in this case, in agreement with better classification results and lower degrees of uncertainty when assigning class labels. Further investigation is required to identify the spatial features that add most value against dimensionality, thereby formulating the next input database of 12 spectral and 4 spatial indices (excluding the MSAVI-based texture). In comparison with the database of 17 input features (Table 6), entropy measures for classes such as Buildings, Clay Soil, Lawn Tennis Court, Red Synthetic Ground and Synthetic Sports Surface was lower than the input database of 17 features. For the same classes, there was also an improvement in classification accuracy (UA). The Road class was identified when the input features were reduced from 17 to 16, also with a low entropy and high (UA) accuracy. Some of the classes (Vineyard and Forest classes) saw an increase in entropy, but also an increase in classification accuracy.

Conversely, the Water class showed an increase in entropy and a decrease in classification accuracy. The MSAVI-based texture index formulated from the MSAVI spectral index was initially added to the input database to distinguish between vegetation classes. However, the overall classification accuracy is the best of the many combinations of inputs to the classifier, thereby confirming the value of the remaining texture indices (Table 4). The Second Moment spatial index, derived from Coniferous Forest spectral index, provided information sufficient to distinguish the Grass and Forest classes and to simultaneously improve their classification accuracy. Only four classes could not be identified using PCM and the 16 feature input database, and an overall improvement of accuracy was achieved.

In order to test the significance of the remaining four spatial indices, various combinations of usage were tested. The only significant result was achieved when using 15 features (excluding MSAVI-based Second Moment and Black Roof Entropy texture measures) which achieved an overall classification accuracy of 72%.

6 Conclusions and Future Work

Our results show that spectral and spatial indices can be combined for classification. The use of spectral and spatial information improves the accuracy of the classifier, but the input dataset must be evaluated to find the best possible combination of indices. We find that every dataset is unique, and the assessment of knowledge-based dimensionality reduction requires an understanding of the specific class that needs to be identified.

Future research could proceed in the following directions:

1. Evaluating the application of object-oriented classification because it accommodates both spectral and spatial information.

2. A few of the classes were not classified regardless of the combination of inputs for the classifier. Although this has been attributed to the smaller spatial distribution of pixels corresponding to these classes, their contribution to this classification approach could be evaluated by considering a different study area that has a higher distribution of such classes.

3. The optimal choice of hyperspectral bands is an ongoing domain of research, e.g. the selection of optimal bands for agricultural crop characteristics using field-collected biophysical variables.[62] For specific classes, an automated method that identifies optimal bands could be developed.

Acknowledgments

We would like to thank Dr.Sc.Nat. Andreas Hueni (University of Zurich) for his assistance during the analysis of the imagery and the related ground truth information. We would also like to thank Dr Richard Twyman for his assistance in the drafting and presentation of the paper. The current paper is adopted and improved from Kallepalli *et al* 2016.[65]

References

1 S.-E. Qian and G. Chen, "A new nonlinear dimensionality reduction method with application to hyperspectral image analysis," 270–273, IEEE International (2007).

2 T. M. Lillesand, R. W. Kiefer, and J. W. Chipman, *Remote Sensing and Image Interpretation*, John Wiley and Sons (Asia) Pte. Ltd., Singapore, Sanjeev Offset Printers, Delhi, 5th ed.

3 C. R. da Silva, J. A. S. Centeno, and S. R. Aranha, "Reduction of the dimensionality of hyperspectral data for the classification of agricultural scenes," (2008).

4 G. Vane and A. F. Goetz, "Terrestrial imaging spectroscopy," *Remote Sensing of Environment* **24**(1), 1–29 (1988).

5 G. Hughes, "On the mean accuracy of statistical pattern recognizers," *IEEE Transactions on Information Theory* **14**, 55–63 (1968).

6 A. Kallepalli, A. Kumar, and K. Khoshelham, "Entropy based determination of optimal principal components of Airborne Prism EXperiment (APEX) imaging spectrometer data for improved land cover classification," *The International Archives of Photogrammetry, Remote Sensing and Spatial Information Sciences* **40**(8), 781 (2014).

7 J. C. Harsanyi and C.-I. Chang, "Hyperspectral image classification and dimensionality reduction: An orthogonal subspace projection approach," *Geoscience and Remote Sensing, IEEE Transactions on* **32**(4), 779–785 (1994).

8 A. Kallepalli, "Spectral and spatial indices based Specific class identification from Airborne Hyperspectral data," Master's thesis, Faculty of Geo-information Science and Earth Observation (ITC), University of Twente (2014).

9 A. Swatantran, R. Dubayah, D. Roberts, *et al.*, "Mapping biomass and stress in the Sierra Nevada using lidar and hyperspectral data fusion," *Remote Sensing of Environment* **115**, 2917–2930 (2011).

10 M. A. Cochrane, "Using vegetation reflectance variability for species level classification of hyperspectral data," *International Journal of Remote Sensing* **21**(10), 2075–2087 (2010).

11 G. Lu and B. Fei, "Medical hyperspectral imaging: a review," *Journal of Biomedical Optics* **19**(1) (2014).

12 J. M. Van Campenhout, "On the peaking of the Hughes mean recognition accuracy: the

resolution of an apparent paradox," *Systems, Man and Cybernetics, IEEE Transactions on* **8**(5), 390–395 (1978).

13 I. T. Jolliffe, *Principal Component Analysis*, Springer, New York (2002).

14 C. Rodarmel and J. Shan, "Principal component analysis for hyperspectral image classification," *Surveying and Land Information Science* **62**(2), 115–122 (2002).

15 A. A. Green, M. Berman, P. Switzer, *et al.*, "A transformation for ordering multispectral data in terms of image quality with implications for noise removal," *IEEE Transactions on Geoscience and Remote Sensing* **26**, 65–74 (1988).

16 A. Plaza, P. Martinez, J. Plaza, *et al.*, "Dimensionality reduction and classification of hyperspectral image data using sequences of extended morphological transformations," *IEEE Transactions on Geoscience and Remote Sensing* **43**, 466–479 (2005).

17 A. Jain and D. Zongker, "Feature selection: Evaluation, application, and small sample performance," *Pattern Analysis and Machine Intelligence, IEEE Transactions on* **19**(2), 153–158 (1997).

18 A. Gillespie, M. Smith, J. Adams, *et al.*, "Interpretation of residual images: spectral mixture analysis of AVIRIS images, Owens Valley, California," in *Proceedings of the 2nd airborne visible/infrared imaging spectrometer (AVIRIS) workshop*, 243–270, NASA Jet Propulsion Laboratory Pasadena, CA (1990).

19 S. B. Serpico and G. Moser, "Extraction of spectral channels from hyperspectral images for classification purposes," *IEEE Transactions on Geoscience and Remote Sensing* **45**, 484–495 (2007).

20 J. R. Jensen, "Biophysical remote sensing," *Annals of the Association of American Geographers* **73**(1), 111–132 (1983).

21 R. M. Haralick, K. Shanmugam, *et al.*, "Textural features for image classification," *IEEE Transactions on Systems, Man, and Cybernetics* (6), 610–621 (1973).

22 J. Estes, E. Hajic, and T. L.R., "Fundamentals of image analysis: Analysis of visible and thermal infrared data.," in *Manual of Remote Sensing*, R. Colwell, Ed., **1**, 987–1124, American Society of Photogrammetry, 2 ed. (1983).

23 P. R. Wolf and B. A. Dewitt, *Elements of Photogrammetry: with applications in GIS*, vol. 3, McGraw-Hill New York (2000).

24 C. F. Jordan, "Derivation of leaf-area index from quality of light on the forest floor," *Ecology* **50**(4), 663–666 (1969).

25 S. Keyworth, M. Jarman, and K. Medcalf, "Assessing the extent and severity of erosion on the upland organic soils of Scotland using earth observation - A GIFTSS implementation test," tech. rep., Environment Systems Limited (2009).

26 G.-R. Liu, C.-K. Liang, T.-H. Kuo, *et al.*, "Comparison of the NDVI, ARVI and AFRI Vegetation Index, along with their relations with the AOD using SPOT 4 vegetation data," *Terrestrial Atmospheric and Oceanic Sciences* **15**(1), 15–32 (2004).

27 J. W. Rouse, Jr., R. H. Haas, J. A. Schell, *et al.*, "Monitoring Vegetation Systems in the Great Plains with ERTS," *NASA Special Publication* **351**, 309 (1974).

28 A. R. Huete, "A soil-adjusted vegetation index (SAVI)," *Remote sensing of environment* **25**(3), 295–309 (1988).

29 G. A. Carter, W. G. Cibula, and T. R. Dell, "Spectral reflectance characteristics and digital imagery of a pine needle blight in the south-eastern United States," *Canadian Journal of Forest Research* **26**(3), 402–407 (1996).

30 J. Vogelmann, B. Rock, and D. Moss, "Red edge spectral measurements from sugar maple leaves," *Remote Sensing* **14**(8), 1563–1575 (1993).

31 A. A. Gitelson and M. N. Merzlyak, "Remote estimation of chlorophyll content in higher plant leaves," *International Journal of Remote Sensing* **18**(12), 2691–2697 (1997).

32 D. Haboudane, J. R. Miller, E. Pattey, *et al.*, "Hyperspectral vegetation indices and novel algorithms for predicting green LAI of crop canopies: Modeling and validation in the context of precision agriculture," *Remote Sensing of Environment* **90**(3), 337–352 (2004).

33 N. H. Broge and E. Leblanc, "Comparing prediction power and stability of broadband and hyperspectral vegetation indices for estimation of green leaf area index and canopy chlorophyll density," *Remote sensing of environment* **76**(2), 156–172 (2001).

34 C. Daughtry, C. Walthall, M. Kim, *et al.*, "Estimating corn leaf chlorophyll concentration from leaf and canopy reflectance," *Remote sensing of Environment* **74**(2), 229–239 (2000).

35 J. Qi, A. Chehbouni, A. Huete, *et al.*, "A modified soil adjusted vegetation index," *Remote sensing of environment* **48**(2), 119–126 (1994).

36 C. D. Elvidge and Z. Chen, "Comparison of broad-band and narrow-band red and near-infrared vegetation indices," *Remote sensing of environment* **54**(1), 38–48 (1995).

37 C. J. Tucker, "Red and photographic infrared linear combinations for monitoring vegetation," *Remote sensing of Environment* **8**(2), 127–150 (1979).

38 A. J. Richardson and C. Wiegand, "Distinguishing vegetation from soil background information [by gray mapping of Landsat MSS data]," (1977).

39 M. S. Kim, *The Use of Narrow Spectral Bands for Improving Remote Sensing Estimations of Fractionally Absorbed Photosynthetically Active Radiation (fapar)* (1994).

40 P. J. Zarco-Tejada, J. R. Miller, T. L. Noland, *et al.*, "Scaling-up and model inversion methods with narrowband optical indices for chlorophyll content estimation in closed forest canopies with hyperspectral data," *IEEE Transactions on Geoscience and Remote Sensing* **39**(7), 1491–1507 (2001).

41 J. Peñuelas, J. Gamon, A. Fredeen, *et al.*, "Reflectance indices associated with physiological changes in nitrogen-and water-limited sunflower leaves," *Remote Sensing of Environment* **48**(2), 135–146 (1994).

42 P. J. Zarco-Tejada, J. Miller, A. Morales, *et al.*, "Hyperspectral indices and model simulation for chlorophyll estimation in open-canopy tree crops," *Remote sensing of environment* **90**(4), 463–476 (2004).

43 P. J. Zarco-Tejada, A. Berjón, R. López-Lozano, *et al.*, "Assessing vineyard condition with hyperspectral indices: Leaf and canopy reflectance simulation in a row-structured discontinuous canopy," *Remote Sensing of Environment* **99**(3), 271–287 (2005).

44 A. Hall, D. Lamb, B. Holzapfel, *et al.*, "Optical remote sensing applications in viticulture-a review," *Australian Journal of Grape and Wine Research* **8**(1), 36–47 (2002).

45 J. Gamon, J. Penuelas, and C. Field, "A narrow-waveband spectral index that tracks diurnal changes in photosynthetic efficiency," *Remote Sensing of environment* **41**(1), 35–44 (1992).

46 A. A. Gitelson, Y. Zur, O. B. Chivkunova, *et al.*, "Assessing carotenoid content in plant leaves with reflectance spectroscopy," *Photochemistry and photobiology* **75**(3), 272–281 (2002).

47 Y. Zha, J. Gao, and S. Ni, "Use of normalized difference built-up index in automatically mapping urban areas from TM imagery," *International Journal of Remote Sensing* **24**(3), 583–594 (2003).

48 B.-C. Gao, "NDWI-A normalized difference water index for remote sensing of vegetation liquid water from space," *Remote sensing of environment* **58**(3), 257–266 (1996).

49 M. Herold, H. Couclelis, and K. C. Clarke, "The role of spatial metrics in the analysis and modeling of urban land use change," *Computers, Environment and Urban Systems* **29**, 369–399 (2005).

50 D. A. Clausi, "An analysis of co-occurrence texture statistics as a function of grey level quantization," *Canadian Journal of remote sensing* **28**(1), 45–62 (2002).

51 B. Datt, T. McVicar, T. Van Niel, *et al.*, "Preprocessing EO-1 Hyperion hyperspectral data to support the application of agricultural indexes," *IEEE Transactions on Geoscience and Remote Sensing* **41**, 1246–1259 (2003).

52 K. I. Itten, F. DellEndice, A. Hueni, *et al.*, "APEX - the Hyperspectral ESA Airborne Prism Experiment," *Sensors* **8**, 6235–6259 (2008).

53 D. Schlapfer, M. Schaepman, S. Bojinski, *et al.*, "Calibration and validation concept for the airborne prism experiment (APEX)," *Canadian journal of remote sensing* **26**(5), 455–465 (2000).

54 A. Hueni, J. Biesemans, K. Meuleman, *et al.*, "Structure, components, and interfaces of the

airborne prism experiment (APEX) processing and archiving facility," *IEEE Transactions on Geoscience and Remote Sensing* **47**(1), 29–43 (2009).

55 M. Jehle, A. Hueni, A. Damm, *et al.*, "APEX-current status, performance and validation concept," 533–537 (2010).

56 "APEX Open Science Data Set Leaflet," (2011).

57 "SwissTopo Web Portal." http://map.geo.admin.ch/?topic=ech&lang=en&X=257116.37&Y=664823.41&zoom=6&bgLayer=ch.swisstopo.swissimage. [Online; accessed 2016-08-08].

58 "Free Data Cubes - APEX - Airborne Prism EXperiment." http://www.apex-esa.org/content/free-data-cubes. [Online; accessed 2016-08-06].

59 M. A. Cho and A. K. Skidmore, "A new technique for extracting the red edge position from hyperspectral data: The linear extrapolation method," *Remote sensing of environment* **101**(2), 181–193 (2006).

60 R. Krishnapuram and J. M. Keller, "A Possibilistic approach to clustering," *IEEE Transactions on Fuzzy Systems* **1**(2), 98–110 (1993).

61 G. M. Foody, "Sub-pixel methods in remote sensing," in *Remote sensing image analysis: Including the spatial domain*, 37–49, Springer (2004).

62 P. S. Thenkabail, R. B. Smith, and E. De Pauw, "Evaluation of narrowband and broadband vegetation indices for determining optimal hyperspectral wavebands for agricultural crop characterization," *Photogrammetric Engineering and Remote Sensing* **68**(6), 607–622 (2002).

63 P. S. Thenkabail, R. B. Smith, and E. De Pauw, "Hyperspectral vegetation indices and their

relationships with agricultural crop characteristics," *Remote Sensing of Environment* **71**(2), 158–182 (2000).

64 J. Penuelas, I. Filella, C. Biel, *et al.*, "The reflectance at the 950–970nm region as an indicator of plant water status," *International Journal of Remote Sensing* **14**(10), 1887–1905 (1993).

65 A. Kallepalli, A. Kumar, K. Khoshelham, *et al.*, "Application of spectral and spatial indices for specific class identification in Airborne Prism EXperiment (APEX) imaging spectrometer data for improved land cover classification," in *Proceedings in SPIE 10005, Earth Resources and Environmental Remote Sensing/GIS Applications VII*, U. Michel, K. Schulz, M. Ehlers, *et al.*, Eds., (Edinburgh, Scotland) (2016).

Ir Akhil Kallepalli is a research student, currently pursuing his PhD in optical imaging and laser systems applications with the Centre for Electronics Warfare, Cranfield University, based in Shrivenham, UK at the Defence Academy of the UK. He received his B. Tech. from Andhra University (2012) and MSc through a joint program between Indian Institute of Remote Sensing and ITC, University of Twente (2014). His current research interests include biomedical applications of lasers, hyperspectral image processing and coastal change detection. He is a current student member of SPIE.

Dr Anil Kumar is a Scientist/Engineer with the Indian Institute of Remote Sensing, Dehradun, India. He received his B. Tech. from University of Lucknow (1992), M. Engg. (1997) and PhD (2007) from IIT Roorkee. Working in the Photogrammetry and Remote Sensing Department, his fields of expertise are Soft Computing, Application for temporal images in specific class Identification, Digital Photogrammetry, Global Positioning System, LiDAR.

Dr Kourosh Khoshelham is a Lecturer at the Department of Infrastructure Engineering of the University of Melbourne. He received an MSc from the University of Tehran (2000); PhD at the Hong Kong Polytechnic University (2004). Dr Khoshelham worked at the University of Tehran, Delft University of Technology and ITC Faculty of Geo-Information Science and Earth Observation of the University of Twente, before moving to Melbourne in February 2015. His research interests include mobile mapping, indoor mapping, building information modelling, UAV photogrammetry and information extraction from point clouds.

Dr David B James is a Senior Lecturer and Head of the Sensors Group in the Centre for Electronic Warfare. He joined MoD in 1989 and worked on non-linear optical systems and devices, gaining a PhD from the Royal Military College of Science in 2002. In 2008, he joined Cranfield University, conducting research into novel laser applications.

Prof Mark A Richardson is Professor of Electronic Warfare and is the Director of Research for Cranfield Defence and Security. He has a first class BSc, an MSc with distinction and a PhD. He is an Associate of the Royal College of Science, has a Diploma of Imperial College, is an Accredited Senior Imaging Scientist and is a Fellow of the Royal Photographic Society. His research interests lies within the use of electro-optics and infrared (EOIR) for electronic warfare, countermeasures, seekers, surveillance and target acquisition systems, man-portable air-defence systems (MANPADs), laser systems, digital image processing, electro-optical protective measures (EOPM) and electro-optical countermeasures (EOCM).

List of Figures

List of Tables

2 Spectral indices database chosen for classification input; 20 classes are identified in these indices, as some indices identify more than 1 class. Note that the band numbers correspond to APEX OSD data

3 Conflicting classes from identified spectral keys

4 Selected texture measures (spatial indices) for input to the classifier

5 Entropy determination and classification results when using the optimally chosen principal components (7 PCs) and only the spectral indices as input for the classifier. The symbol '/' indicates that the class was not identified in the classification process.

6 Entropy determination and classification results when using the Indices and Textures database (17 and 16 features) as input for the classifier. The symbol '/' indicates that the class was not identified in the classification process.

7 Entropy determination and classification results when using the Indices and Textures database (15 features) as input for the classifier. The symbol '/' indicates that the class was not identified during the classification process.